An Experimental and Theoretical Evaluation of the Reactions of Silver Hyponitrite with Phosphorus Halides. In Search of the Elusive Phosphorus-Containing Hyponitrites

Hyun Joo, M. A. Salam Biswas,† William E. Hill,* and Michael L. McKee*

Department of Chemistry and Biochemistry, Auburn University, Auburn, Alabama 36849

Received: September 6, 2004; In Final Form: November 15, 2004

In the reaction of F_2PBr, $F_2P(O)Br$, $(C_6F_5)_2PBr$, $(CH_3)_2P(S)Br$, and $(CH_3)_2P(O)Cl$ with silver hyponitrite ($AgON{=}NOAg$), nitrous oxide (N_2O) and μ-oxo phosphorus species were obtained in all cases rather than the plausible hyponitrite alternative. Theoretical calculations of the geometries and expected decomposition pathways of the phosphorus-containing hypothetical hyponitrites were carried out at the B3LYP/6-311+G-(2df)//B3LYP/6-31+G(d) level. The *cis*-hyponitrite, $XON{=}NOX$ ($X{=}PF_2$, OPF_2), is predicted to concertedly decompose to N_2 plus phosphorus-containing radicals (OPF_2, O_2PF_2) or to N_2O plus the μ-oxo phosphorus species, X−O−X, ($X{=}PF_2$, OPF_2) with the former pathway having a smaller activation barrier (4.6 kcal/mol, $X{=}PF_2$; 10.5 kcal/mol, $X{=}OPF_2$). On the other hand, *trans*-hyponitrite can only decompose to N_2 plus the phosphorus-containing radicals, because there is a very high barrier for rearrangement to *cis*-hyponitrite. These results are in disagreement with experiment, because only the μ-oxo phosphorus species are observed. Reconciliation between experiment and theory is made for $X{=}OPF_2$ when a silver cation is included in the calculations. In THF (as a model for neat $F_2P(O)Br$), the silver cation is predicted to reverse the order of the two transition states through stronger interactions with the oxygen atoms in the transition state of the N_2O-producing pathway. Thus, Ag(I) is predicted to be not only catalytic for $X{=}OPF_2$ but also product-specific toward the μ-oxo products.

Introduction

The existence of organic hyponitrites is well-documented in the chemical literature. These hyponitrites have been synthesized by reactions of appropriate organic halides and silver hyponitrite.[1−3] The hyponitrites are a source of alkoxy or aryoxy radicals. The geometries of alkyl hyponitrites are trans-based on vibrational spectroscopy,[4,5] dipole moment measurements,[6] and low-temperature X-ray crystallography.[7] Decomposition is thought to occur by homolytic scission with the loss of N_2.[8−10]

The presence of the N=N bond has been confirmed by its ultraviolet spectrum.[11] The trans isomer has been found to be the product obtained by usual preparative methods as confirmed by Raman[12−14] and infrared[15−17] spectroscopy. *Cis*-hyponitrous acid has been postulated as an unstable intermediate in the reaction of hydroxylamine and nitrous acid[18] and in the reduction of nitrous acid by europium(II).[19]

A number of alkali metal, alkaline earth metal, mercury, silver, and lead hyponitrites have been synthesized. Mercury and silver hyponitrites are known to have a trans configuration,[4] while sodium hyponitrite has been synthesized in both the cis and trans geometries.[20,21] Several transition metal hyponitrites have been prepared, including the very interesting [Ni(dppf)-N_2O_2], [Pd(dppe)N_2O_2], and [Pt(dppf)N_2O_2] hyponitrites, all of which have *cis*-hyponitrite geometries and decompose by unimolecular kinetics.[21,22]

Beck et al.[13] reported that the decomposition of triphenyltin hyponitrite, $Ph_3SnON{=}NOSnPh_3$, yielded N_2O and $(Ph_3Sn)_2O$. On the other hand, Wiberg et al.[14] prepared trimethylsilyl hyponitrite, $Me_3SiON{=}NOSiMe_3$, and reported that thermolysis gave N_2, trimethylsilanol, and hexamethyl disiloxane.

Phosphorus-containing hyponitrites are conspicuous by their absence in the chemical literature. Furthermore, no attempts to synthesize these potentially interesting molecules have been reported. This is in spite the potential use of such hyponitrites to generate extremely interesting radicals (e.g., F_2PO, F_2PO_2, $F_2P(S)O$). The current work deals with the attempts to prepare such hyponitrites by reaction with silver hyponitrite as shown in the following equation (eq 1):

$$2R_2P(Y)X + AgON{=}NOAg \rightarrow 2AgX + R_2P(Y)ON{=}NOP(Y)R_2 \quad (1)$$

$$(R = CH_3, F;\ Y = O, S;\ X = \text{halide})$$

In the thermal decomposition of hyponitrites, the experimental evidence suggests that *trans*-hyponitrites decompose to N_2 plus other products, while *cis*-hyponitrites may decompose to N_2O plus products.[23] A related issue is whether the decomposition is concerted (eq 2a) or stepwise (eq 2b).

$$RON{=}NOR \rightarrow 2RO^{\bullet} + N_2 \quad (2a)$$

$$RON{=}NOR \rightarrow RO^{\bullet} + {}^{\bullet}N{=}NOR \rightarrow 2RO^{\bullet} + N_2 \quad (2b)$$

Neuman and Bussey determined the activation volume of the *trans*-di-*tert*-butyl hyponitrite decomposition and suggested the reaction follows the concerted pathway.[10] For *trans*-hyponitrites, structural and mechanistic studies are well-established.[20,24] On the contrary, mechanistic studies on *cis*-hyponitrites are rare.[22]

* Corresponding authors.
† Current address: Chemistry Department, Tuskegee University, Tuskegee, AL 36088.

10.1021/jp045984j CCC: $30.25
Published on Web 01/22/2005

To understand the different chemical reactivities of *trans*- and *cis*-hyponitrites, theoretical calculations were carried out. No previous calculations have been reported on the structures, stabilities, or decomposition reaction pathways of phosphorus-containing hyponitrites. Hybrid density functional theory, B3LYP, has been applied to study the decomposition pathways of XON=NOY (X, Y = PF_2, OPF_2) to establish the probable reaction mechanisms leading to the observed final products.

Experimental Section

Standard vacuum-line techniques were used to purify and transfer all volatile substances. Nonvolatile compounds were handled in a nitrogen-filled glovebag containing P_4O_{10} as a desiccant.

Infrared spectra were determined on a Perkin-Elmer 983 spectrophotometer. Liquids were examined as neat samples; solids were studied as Nujol and fluorolube mulls. ^{31}P and ^{1}H NMR spectra were obtained at 162 and 400 MHz on a Bruker AM 400 spectrometer. ^{31}P chemical shifts were measured relative to H_3PO_4 (85%, external) and ^{1}H relative to TMS (internal). Mass spectra were recorded on a Finnigan 3300 mass spectrometer equipped with a gas inlet system and a solid probe.

Gaseous reactants were obtained from Matheson. Toluene and benzene (dried over sodium) and acetonitrile (purified by distillation over phosphorus pentoxide and collected over molecular sieves) were obtained from Fisher. Thiophosphoryl chloride was obtained from Aldrich and distilled prior to use. Bromopentafluorobenzene was obtained from Columbia Organics and dried over 4A molecular sieves prior to use. Phosphorus trichloride was obtained from Matheson, Coleman & Bell and distilled prior to use. Silver hyponitrite was prepared by the literature method.[25] $(CH_3)_2P(S)Br$,[26,27] $(CH_3)_2P(O)Cl$,[28] $F_2P(O)Br$,[29] $(C_6F_5)_2PBr$,[30] and F_2PBr[31] were prepared by literature methods.

Reaction of Dimethylthiophosphinic Bromide with Silver Hyponitrite in 2:1 Ratio. $(CH_3)_2P(S)Br$ (0.462 g, 2.67 mmol) was placed in a 100 mL three-necked flask containing a magnetic stirring bar. Toluene (30 mL) was added to the flask to dissolve the bromide. Silver hyponitrite (0.382 g, 1.38 mmol) was placed in a thumb-shaped solid addition tube and added slowly over a period of 15 min at room temperature. The system was protected from light by wrapping the flask with aluminum foil. The collected gas (1.33 mmol) was shown to be N_2O by its infrared and mass spectra. The yellowish liquid was filtered off, and the solvent was removed in vacuo to give 0.269 g of solid, identified as $(CH_3)_2P(S)OP(S)(CH_3)_2$ by its ^{31}P NMR and infrared spectrum.

Several low-temperature reactions were carried out to see if any hyponitrite, $(CH_3)_2P(S)ON=NO(S)P(CH_3)_2$, could be detected. In one of those reactions, 0.219 g (1.27 mmol) of dimethylthiophosphinic bromide was taken in a 100 mL flask as described in the previous reaction, using 25 mL of toluene and 0.205 g (0.74 mmol) of silver hyponitrite. The reaction flask was placed in a dry ice acetone slush bath to keep the reaction mixture at −78 °C. The silver hyponitrite was then added slowly over a 10 min period. After 20 min, no volatiles were observed. The reaction flask was then quickly transferred to a chlorobenzene−liquid nitrogen slush bath (−45 °C). Again, no gas was detected after 20 min. The reaction flask was then transferred to a carbon tetrachloride−liquid nitrogen slush bath (−23 °C). After 20 min, 2 Torr (V = 396 mL) of pressure was observed. The color of the reaction mixture did not change. The reaction flask was then transferred to an ice bath. After a while, the pressure observed was 13 Torr (V = 396 mL). The reaction went to completion at this temperature. In the second batch, the reaction was monitored by ^{31}P NMR on a Bruker AM 400 instrument at −30 °C, using 0.0981 g (0.47 mmol) of the bromide. From the previous low-temperature reaction, it was thought that the reaction might have started well below −23 °C. Therefore, the reactants were mixed at bromobenzene−liquid nitrogen temperature (−30 °C). The amount of silver hyponitrite taken was 0.079 g (0.03 mmol). After mixing the reactants for 20 min, a 2 mL portion of the solution was transferred by a syringe into an NMR tube, and the spectrum was recorded at −30 °C. Two peaks were found at 66.0 and 91.3 ppm. These peaks were assigned to dimethylthiophosphinic bromide and $(CH_3)_2P(S)OP(S)(CH_3)_2$, respectively.[32] The reaction was allowed to go for 6 h. Again, a 2 mL portion of the liquid from the flask was withdrawn by syringe, and the ^{31}P NMR spectrum was taken at −30 °C. Only one peak was observed at 91.3 ppm, which corresponds to the chemical shift of phosphorus in $(CH_3)_2P(S)OP(S)(CH_3)_2$.

The mass spectrum of the solid product showed the following peaks: $M^+ = [(CH_3)_2P(S)OP(S)(CH_3)_2^+]$ 202 (44%); $(M - CH_3)^+$ 187 (3%); $(M - HS)^+$ 169 (27%); $(M - CH_3{-}S)^+$ 155 (3%); $(CH_3)_2P(S)OH^+$ 110 (7%); $(CH_3)_2PS^+$ 93 (100%); $H_2C{=}PS^+$ 77 (58%); PS^+ 63 (45%); PO^+ 47 (77%); PCH_2^+ 45 (51%); CH_3^+ 15 (41%). Mass spectrum of the gaseous product: N_2O^+ 44 (100%); NO^+ 30 (35%).

The infrared spectrum of the gaseous sample is given as follows (all values in cm^{-1}). N_2O: 2234 (s), 2214 (s), 1299 (s), 1272 (s).

Reaction of Dimethylphosphinic Chloride with Silver Hyponitrite in 2:1 Ratio. Dimethylphosphinic chloride (0.331 g, 2.96 mmol) was dissolved in 20 mL of toluene (Na dried) in a 100 mL three-necked flask equipped with a magnetic stirring bar. Silver hyponitrite (0.440 g, 1.60 mmol) was placed in a thumb-shaped tube with ground joint and fitted to the flask. The flask was then evacuated on the vacuum line. The entire flask including the thumb-shaped tube was wrapped with aluminum foil to protect the contents from light. Silver hyponitrite was then added to the solution over a period of 20 min. The heterogeneous mixture was stirred for 2 h at room temperature. The flask was then connected to the vacuum line, and the gaseous product was collected (1.46 mmol) at −196 °C. The gas was shown to be N_2O by infrared and mass spectrometry. The mixture in the three-necked flask was filtered, and the solvent was evaporated from the filtrate under high vacuum. The solid recovered was 0.247 g (98% yield) based on the amount of $(CH_3)_2P(O)Cl$ reacted. The ^{31}P NMR of the solid run in toluene showed only one signal at 49.6 ppm. The mass spectrum of the compound $(CH_3)_2P(O)OP(O)(CH_3)_2$ was: M^+ peak not observed; $(CH_3)_2PO_2H^+$ 94 (41%); $(CH_3)_2P(O)H_2^+$ 79 (100%); HPO^+ 48 (4%); H_2PO^+ 49 (7%); PO_2^+ 63 (3%); $(CH_3)_2P{=}O^+$ 77 (5%). The mass spectrum and the infrared spectrum of the gas collected at −196 °C are identical with the results reported in the preceding section. The infrared spectrum of the solid in Nujol showed the following peaks (all values in cm^{-1}): 1305 (s) (P=O), 972 (vs) (P−O−P, asym.), 871 (s) (P−O−P, sym.), 723 (m) (P−C).

Reaction of Difluorophosphinic Bromide with Silver Hyponitrite in 2:1 Ratio. The reaction of difluorophosphinic bromide was performed in the absence of light. $F_2P(O)Br$ (9.20 mmol) was condensed into a Fisher-Porter tube charged with silver hyponitrite (1.701 g, 6.20 mmol). The mixture was warmed to room temperature and left for 2 h. The product was passed through four traps at −78, −130, −160, and −196 °C. The −78 and −130 °C traps each contained 4.40 mmol of gas

with a liquid mixture of $F_2P(O)Br$ and $F_2P(O)OP(O)F_2$ [33] (as indicated by infrared spectroscopy). There were no products in the −160 °C trap. The −196 °C trap contained 4.0 mmol of a gas identified as N_2O by its mass and infrared spectra. The data are the same as those obtained for N_2O in previous reactions.

The infrared spectrum of the samples from the −78 and −130 °C traps showed the following absorptions (all values in cm^{-1}): 1425 (s) (P═O) $F_2P(O)OP(O)F_2$; 1375 (ms) $F_2P(O)Br$; 1325 (s) $F_2P(O)Br$; 1075 (vs) (POP asym. stretch) $F_2P(O)OP(O)F_2$; 993 (s) (POP sym. stretch) $F_2P(O)OP(O)F_2$; 976 (vs) $F_2P(O)$-$OP(O)F_2$; 942 (vs) $F_2P(O)Br$; 899 (s) $F_2P(O)OP(O)PF_2$; 885 (vs) $F_2P(O)Br$; 560 (vs) $F_2P(O)Br$.

The mass spectra showed the following peaks for the gas in the −130 °C trap: $F_2P(O)Br^+$ 164 (91%), 166 (91%); $FP(O)Br^+$ 145 (37%), 147 (37%); F_3PO^+ 104 (91%); PF_3^+ 88 (21%); F_2PO^+ 85 (100%); PF^+ 50 (35%); PO^+ 47 (71%).

Reaction of Bis(perfluorophenyl)bromophosphine and Silver Hyponitrite in 2:1 Ratio. $(C_6F_5)_2PBr$ (1.171 g, 2.63 mmol) was dissolved in 25 mL of benzene (Na dried) in a three-necked flask. The arrangement and precautions were the same as the previous reactions. Silver hyponitrite (0.376 g, 1.36 mmol) was added slowly over a period of 10 min, and the mixture was stirred for 2 h at room temperature and then filtered. The amount of product, recovered from the filtrate by removing the solvent in vacuo, was 0.956 g. The gas evolved (1.27 mmol) was N_2O, identified by mass spectral and infrared data. The ^{31}P NMR spectrum run in benzene showed a multiplet (apparent nonet) at +93.4 ppm assigned to $(C_6F_5)_2POP(C_6F_5)_2$. The mass spectrum of the white solid, $(C_6F_5)_4P_2O$, was as follows: $(C_6F_5)_4P_2O^+$ 746 (30%); $C_{24}F_{19}P_2O^+$ 727 (3%); $(C_6F_5)_3P_2O^+$ 579 (11%); $(C_6F_5)_3P^+$ 532 (25%); $(C_6F_5)_2PO^+$ 381 (92%); $(C_6F_5)_2P^+$ 365 (50%); $C_{12}F_8^+$ 296 (100%); $C_{12}F_7^+$ 277 (11%); $C_6F_5PF^+$ 217 (58%); $C_6F_5P^+$ 198 (22%); $C_6F_4P^+$ 179 (15%); $C_6F_4^+$ 148 (20%); $C_6F_3^+$ 129 (95%); $C_5F_3^+$ 117 (35%); CF_3^+ 69 (100%); PO^+ 47 (8%). The infrared spectrum showed two intense peaks at 909 and 640 cm^{-1} (P—O—P asym. and sym.). The absorptions at 1465 (s) and 1102 (s) cm^{-1} are P—C stretching modes, while the bands at 1377 (s), 1303 (s), and 1232 (s) cm^{-1} are C—F stretching bands. The N_2O gas was identified as previously described.

Reaction of Bromodifluorophosphine and Silver Hyponitrite in 2:1 Ratio. Silver hyponitrite (1.701 g, 6.2 mmol) was placed in a Fisher-Porter tube wrapped in aluminum foil. F_2PBr gas (12.4 mmol) was condensed into the tube. The mixture was warmed to room temperature and kept for 2 h. The reactor contents were passed through −90, −130, −160, and −196 °C traps. Nothing was collected in the −90 °C trap. The −130 °C trap contained 5.4 mmol of gas. The infrared spectrum showed it to be a mixture of F_2POPF_2 [34] and F_2PBr. The −160 °C trap stopped 4.1 mmol of gas, which was identified as N_2O from its infrared and mass spectrum. The mass spectrum of the products collected in the −130 °C trap was as follows: $F_2POPF_2^+$ 154 (60%); F_2POPF^+ 135 (23%); F_3PO^+ 104 (13%); F_2PO^+ 85 (33%); PF_2^+ 69 (29%); PF^+ 50 (65%); PO^+ 47 (49%); P^+ 31 (4%); F_2PBr^+ 148 (96%); F_2PBr^+ 150 (100%); $FPBr^+$ 129 (29%); $FPBr^+$ 131 (23%). The mass spectrum of the −160 °C trap gas was as follows: $F_2POPF_2^+$ 154 (37%); F_3PO^+ 104 (33%); F_2PO^+ 85 (41%); PF_2^+ 69 (100%); PF^+ 50 (31%); PO^+ 47 (46%); N_2O^+ 44 (85%).

Computational Methods

The decomposition of the three phosphorus-containing hyponitrite species listed in Scheme 1 (**A**, **B**, **C**), where **A** and **C** were the synthetic targets of our experimental study, were considered in our computational study (numbering system is given for **C**). Hyponitrite **B** was included to examine the effects of asymmetric oxygen substitution on phosphorus. The *Gaussian 03* program package[35] was used for all calculations. The density functional method was used with the B3LYP choice exchange and correlation functionals, which has been shown to yield good results for a number of inorganic systems.[36] For geometry optimization, the 6-31+G(d) basis set was used for F, N, O, and P atoms, and the LANL2DZ[37] effective core potential (ECP) and basis set was used for the Ag^+ ion. For transition states with strong biradical character, we applied the unrestricted broken-symmetry UB3LYP method with the same basis set. At every optimized geometry, frequency calculations were made using the same level of theory to characterize the stationary points as minima (0 imaginary frequencies) or transition states (1 imaginary frequency). The transition vector of every transition state (TS) structure was animated with the MOLDEN program.[38] If necessary, intrinsic reaction coordinates (IRC) were calculated to connect a TS to the corresponding minima. After the reaction profile was constructed, single-point calculations were performed on stationary points with the larger 6-311+G(2df) basis set for F, N, O and P and the standard SDD[39] effective core potential and basis set for Ag. For convenience, "SBS" was used to indicate B3LYP/6-31+G(d)+LANL2DZ and "LBS" to indicate B3LYP/6-311+G(2df)+SDD. The natural population analysis (NPA) charges were obtained by using the NBO[40] program implemented in the Gaussian program.

SCHEME 1

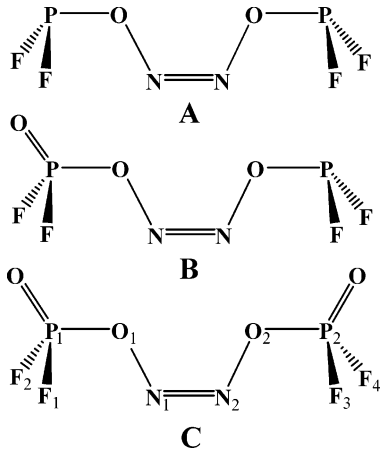

The reactions of F_2PBr and $F_2P(O)Br$ with AgON═NOAg were carried out in neat liquid. To estimate the effect of the medium, single-point energy calculations were carried out using the conductor polarizable continuum model (CPCM)[41] at the B3LYP/6-311+G(2df) level with the dielectric constant of tetrahydrofuran (THF). While the dielectric constants of F_2PBr and $F_2P(O)Br$ are unknown, the dielectric constant of Cl_3PO is known to be 14.0, which is reasonably close to that of THF (7.58).[42]

The structures and geometrical parameters of $F_2PON═NOPF_2$ (**A**), $F_2P(O)ON═NOPF_2$ (**B**), and $F_2P(O)ON═NOP(O)F_2$ (**C**) species are given in Figure 1. Relative energies, enthalpies, and free energies (kcal/mol) at the B3LYP/LBS//B3LYP/SBS level of theory are given for **A** in Table 1, for **B** in Table 2, and for **C** in Table 3. A table of spin-squared values, absolute energies, and free energies of solvation in THF is available as Supporting Information (Table S1) as well as Cartesian coordinates of all structures in Tables 1−3 and 5 (Table S2). Reaction profiles of free energies (kcal/mol) at 298 K at the B3LYP/LBS//B3LYP/

SBS level of theory are provided for **A** (Figure 2), **B** (Figure 3), and **C** (Figure 4).

Results and Discussion

The reactions of silver hyponitrite with $(CH_3)_2P(S)Br$, $(CH_3)_2P(O)Cl$, $F_2P(O)Br$, and F_2PBr have been evaluated as potential synthetic paths to the hyponitrites $R_2P(Y)ON{=}NOP(Y)R_2$ (Y = O, S; R = CH_3, F) and $R_2PON{=}NOPR_2$ (R = C_6F_5, F). In all cases, the reactions were carried out in the absence of moisture and light (because silver hyponitrite is light-sensitive). The gaseous products were identified by infrared and mass spectra; the solids were identified by NMR, mass, and infrared spectra. The results obtained in this series of reactions may be expressed by the following general equations (eq 3):

$$2R_2P(Y)X + AgON{=}NOAg \rightarrow 2AgX + N_2O + R_2P(Y)OP(Y)R_2 \quad (3a)$$

(R = CH_3, F; Y = electron pair, O, S; X = halide)

$$2R_2PX + AgON{=}NOAg \rightarrow 2AgX + N_2O + R_2POPR_2 \quad (3b)$$

(R = C_6F_5, F; X = Br)

Thus, no hyponitrites were isolated from the synthetic pathway even when reactions were carried out at low temperatures. In all cases, μ-oxo phosphorus-containing species were obtained. The change in substituents from electron-releasing methyl groups to the highly electronegative F (eq 3a, R = CH_3, F) or from tricoordinate phosphorus to pentavalent phosphorus, P = O or P = S (eq 3a, Y = electron pair, O, S) did not change the reaction pathway. We had hoped that the postulated hyponitrites formed in these reactions might have stability comparable to *tert*-butyl hyponitrite. Because the stability of *tert*-butyl hyponitrite has been attributed to its lack of an α-hydrogen,[2] we reasoned that the proposed hyponitrites of phosphorus might have comparable stability to *tert*-butyl hyponitrite because they also lacked an α-hydrogen.

Cis-hyponitrites are known to be less stable than *trans*-hyponitrites[43,44] and decompose with the elimination of N_2. Therefore, the fact that we do not observe a phosphorus-containing hyponitrite might be due to an initially formed *cis*-hyponitrite (which decomposes) or to the rearrangement of the *trans*-hyponitrite to *cis*-hyponitrite under experimental conditions. It is interesting to note that the electronegative fluorine or less electronegative perfluorophenyl groups on the trivalent phosphorus did not result in an identifiable hyponitrite. To determine whether this might have a thermodynamic or kinetic origin, we turned to theoretical calculations.

Optimized geometries for the hypothetical hyponitrites are shown in Figure 1, and NPA charges are given in Table 4. For all three molecules, the cis isomer has slightly shorter N=N bond lengths (about 0.007 Å) and longer N−O bond lengths, which indicate less π-delocalization in the cis compared to the trans isomer (Figure 1, **AC/AT**, **BC/BT**, **CC/CT**). As the phosphinyl (F_2P) groups in $F_2PON{=}NOPF_2$ are oxidized to phosphoryl ($F_2P(O)$) groups (**AC** → **CC**), the O−P bond lengths are shortened from 1.667 to 1.634 Å. The oxidation to phosphoryl groups makes these phosphorus atoms more positively charged (III → V) and leads to a strong bonding interaction between P_1 and O_1 (See Scheme 1 for numbering). Interestingly, in the unsymmetrical $F_2P(O)ON{=}NOPF_2$ (**BC**), the phosphoryl $P_1{-}O_1$ bond length is much shorter than the phosphinyl $O_2{-}P_2$ bond length (1.623 and 1.680 Å, respectively), while the $O_1{-}N_1$ and $N_2{-}O_2$ bond lengths change in the opposite direction (1.450 and 1.407 Å, respectively) which suggests a resonance contribution from $P_1{=}O_1{\cdots}N_1{=}N_2{=}O_2{\cdots}P_2$.

The elimination of N_2O can occur after the phosphorus-containing group (F_2P or ($F_2P(O)$) has rotated around the N−O bond. This allows interaction between a phosphorus center and a remote oxygen center (i.e., P_2 with O_1 in **AC-1**, **BC-1**, or **CC-1** or P_1 with O_2 in **BC-2**). In **AC-1** and **BC-1**, the interacting phosphorus center is an $-OPF_2$ group which is more electrophilic than an $-OP(O)F_2$ group. As a consequence, the nonbonded $P_2{-}O_1$ interactions in **AC-1** and **BC-1** cause the $O_2{-}P_2$ bond lengths to increase relative to **AC** and **BC** (1.667 → 1.729 Å and 1.680 → 1.756 Å for **AC** → **AC-1** and **BC** → **BC-1**, respectively). In turn, the free energy of activation values for the elimination of N_2O are small for **AC-1** → **AC-TS2** and **BC-1** → **BC-TS2** (7.9 and 1.1 kcal/mol, respectively). On the other hand, in **BC-2** and **CC-1**, the $-OP(O)F_2$ group is the electrophile, which causes a much smaller increase in the P−O bond length relative to **BC** and **CC** (1.623 → 1.646 Å and 1.634 → 1.656 Å for **BC** → **BC-2** and **CC** → **CC-1**, respectively) and leads to a larger free energy of activation for N_2O elimination (21.4, 17.6 kcal/mol for **BC-2** → **BC-TS5**, **CC-1** → **CC-TS2**, respectively).

The transition states for rotation around the N=N bond which interconverts *cis*- and *trans*-hyponitrites (**XCT-TS**, **X** = **A**, **B**, **C**) were located. The transition states, which have strong biradical character ($\langle S^2\rangle$ = 1.01−1.02), are reached after about 92° rotation around the N−N bond, which breaks the N=N π−bond and causes the N−N bond to elongate by about 0.1 Å. The activation enthalpies (298 K) for the cis → trans rearrangement are very similar for **AC**, **BC**, and **CC** (50.7−51.9 kcal/mol, Tables 1−3).

In all three cases, the cis isomers are found to be global minima and trans isomers are about 2 kcal/mol higher in free energy. Their potential energy surfaces are very similar along the free energy reaction coordinates (Figures 2−4). Rotation about the N−O bond in the cis isomer leads to a transition state (**XC-TS1**, **X** = **A**, **B**, **C**) and then an intermediate (**XC-1**, **X** = **A**, **B**, **C**) followed by another barrier (**XC-TS2**, **X** = **A**, **B**, **C**) to yield N_2O plus product.

The cis isomer is predicted not to form the trans isomer due to the high free energy barriers for breaking the N=N bond ((**XCT-TS**, **X** = **A**, **B**, **C**), 51.2−52.5 kcal/mol). We would like to emphasize that these predictions are for unimolecular rearrangement of the cis isomer. It is possible that the coordination of an electrophile to the cis isomer could lower the barrier for cis ↔ trans isomerization. For example, coordination of Ag^+ to nitrogen could lower the barrier for cis ↔ trans isomerization by stabilizing the transition state (Figure 5).

The trans isomers are predicted to undergo concerted synchronous fragmentation (**XT-TS**, **X** = **A**, **B**, **C**) of both N−O bonds to form N_2 plus two radicals. Thus, if a trans isomer is initially formed, it can only fragment to produce N_2, because rearrangement to the cis isomer is blocked by a high barrier (unassisted reaction). On the other hand, the cis isomer can fragment to form either N_2 (with radicals formed) or N_2O (with no radicals formed) with competitive activation free energies (Figures 2−4). For **A** and **C**, the pathway for N_2 production is 4.6 and 10.5 kcal/mol lower than the pathway for N_2O production, while for **B**, the N_2O production pathway is lower than the N_2 production by 3.0 kcal/mol. The N_2O production pathway for **C** is much higher than for **A** or **B**, because only

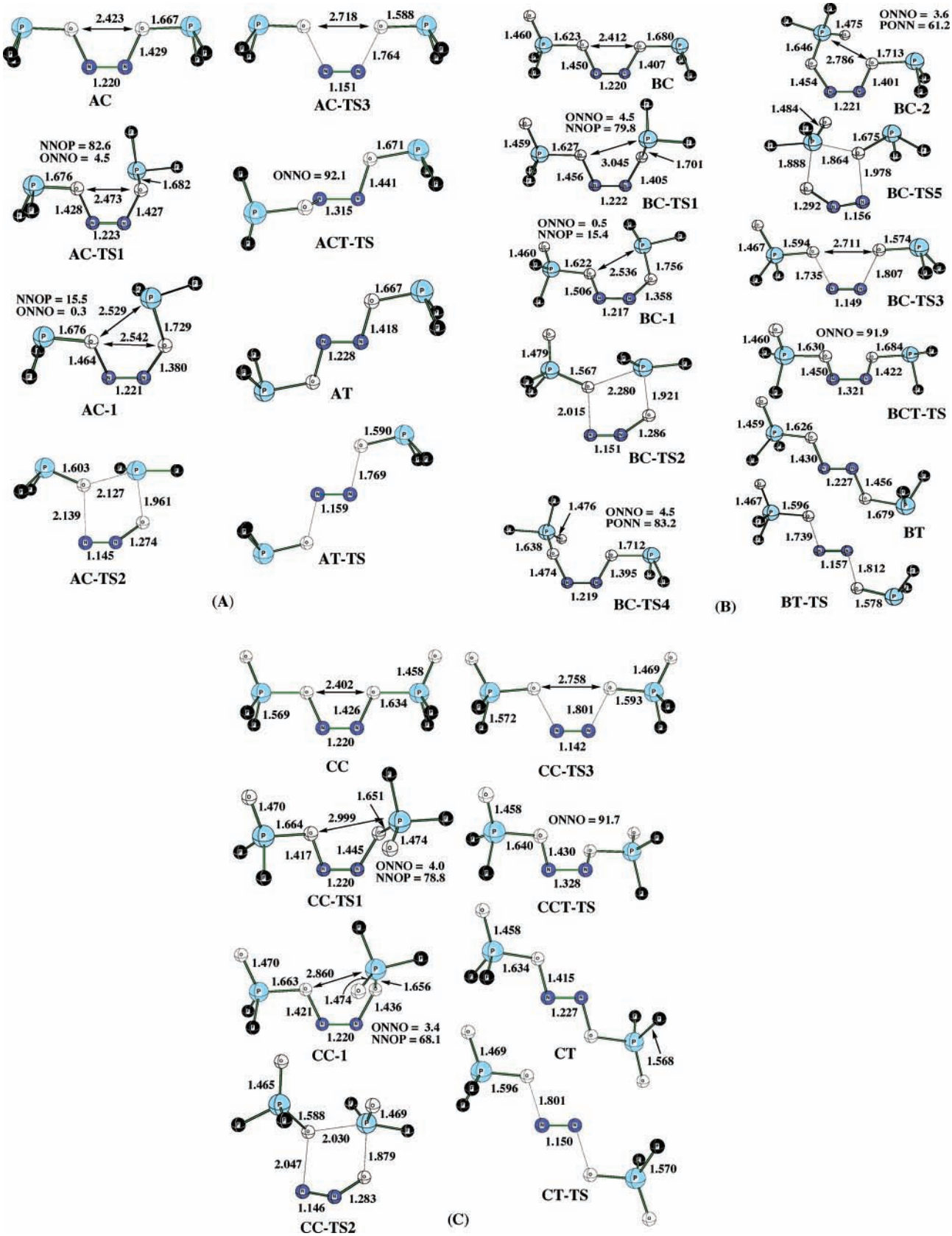

Figure 1. Calculated geometries for species on the following PES: $F_2PON{=}NOPF_2$ (**A**), $F_2P(O)ON{=}NOPF_2$ (**B**), and $F_2P(O)ON{=}NOP(O)F_2$ (**C**) at the B3LYP/SBS level.

the $-OP(O)F_2$ group (not the $-OPF_2$ group) can attack the remote oxygen atom.

Because no radical products are observed for **A** and **C**, the N_2O production pathway must be the preferred pathway under our experimental conditions. If the phosphorus-containing hyponitrite (**A**, **B**, or **C**) is an intermediate in the reaction, this suggests the following: (1) the *cis*-hyponitrite is formed in the reaction, and (2) the *cis*-isomer decomposes via the N_2O

TABLE 1: Relative Enthalpies and Free Energies (kcal/mol) on the Potential Energy Surface of $F_2PON{=}NOPF_2$ at the B3LYP/LBS//B3LYP/SBS Level

	ΔE_e	ΔH_{0K}	ΔH_{298K}	ΔG_{298K}	ΔG_{THF}[a]
AC	0.0	0.0	0.0	0.0	0.0
AC-1	6.0	5.7	5.8	5.7	6.0
AT	1.9	1.9	1.9	1.9	2.2
AC-TS1	6.8	6.6	6.1	7.0	7.5
AC-TS2	14.4	13.3	13.4	13.2	13.9
AC-TS3	11.5	9.1	9.7	7.8	9.3
AT-TS	15.5	13.1	13.9	12.1	13.1
ACT-TS	53.3	50.7	50.7	50.5	51.2
$N_2 + 2OPF_2$	−44.3	−47.3	−46.5	−69.2	−66.2
$N_2O + F_2POPF_2$	−47.4	−48.2	−47.7	−58.3	−55.8

[a] Including solvation free energy calculated by CPCM method in THF.

TABLE 2: Relative Enthalpies and Free Energies (kcal/mol) on the Potential Energy Surface of $F_2P(O)ON{=}NOPF_2$ at the B3LYP/LBS//B3LYP/SBS Level

	ΔE_e	ΔH_{0K}	ΔH_{298K}	ΔG_{298K}	ΔG_{THF}[a]
BC	0.0	0.0	0.0	0.0	0.0
BC-1	6.1	5.8	5.8	6.0	6.6
BC-2[b]	8.5	8.2	8.3	8.3	7.5
BT	2.2	2.2	2.2	2.2	2.2
BC-TS1	7.4	7.1	6.6	7.4	7.9
BC-TS2	9.6	8.5	8.6	8.8	7.7
BC-TS3	14.5	11.9	12.5	10.5	10.9
BC-TS4[b]	8.3	8.0	7.5	8.8	7.8
BC-TS5	30.4	29.5	29.2	30.8	28.9
BT-TS	19.2	16.5	17.1	15.3	15.7
BCT-TS	54.0	51.5	51.5	51.2	49.9
$N_2 + OPF_2 + O_2PF_2$	−26.3	−30.4	−29.4	−51.7	−47.4
$N_2O + F_2POP(O)F_2$	−49.5	−50.2	−49.8	−60.9	−58.6

[a] Including solvation free energy calculated by CPCM method in THF. [b] Geometry optimized at the B3LYP/cc-pVDZ level.

production pathway. While the two pathways (N_2 production and N_2O production) have very similar free energies of

TABLE 3: Relative Enthalpies and Free Energies (kcal/mol) on the Potential Energy Surface of $F_2(O)PON{=}NOP(O)F_2$ at the B3LYP/LBS//B3LYP/SBS Level

	ΔE_e	ΔH_{0K}	ΔH_{298K}	ΔG_{298K}	ΔG_{THF}[a]
CC	0.0	0.0	0.0	0.0	0.0
CC-1[b]	10.0	9.5	9.6	8.5	8.2
CT	2.0	1.9	2.0	1.9	2.1
CC-TS1[b]	9.7	9.1	8.7	9.4	9.3
CC-TS2	29.9	28.9	28.8	29.3	25.8
CC-TS3	19.5	16.5	17.2	15.1	15.3
CT-TS	24.7	21.5	22.2	19.9	16.3
CCT-TS	54.3	51.8	51.9	51.5	52.3
$N_2 + 2O_2PF_2$	−9.7	−15.0	−13.9	−36.7	−30.7
$N_2O + F_2P(O)OP(O)F_2$	−49.8	−50.5	−50.0	−61.7	−59.2

[a] Including solvation free energy calculated by CPCM method in THF. [b] Geometry optimized at the B3LYP/cc-pVDZ level.

activations for **A**, the calculations clearly predict N_2 production for **C**, in conflict with experiment. Thus, the reaction profile of **C** constructed by considering all the thermodynamic corrections and solvation free energies fails to explain the reaction mechanism. The question is why.

The possibility that the silver cation might have a catalytic effect on the decomposition of the *cis*-isomer of **C** was considered. Optimized geometries of silver cation complexes with **C** are given in Figure 6. The most stable Ag(I)−**C** complex is not with **CC** (the global minimum) but rather with **CC-1** due to the much stronger Ag(I) interactions with the P═O oxygens (2.366 and 2.336 Å, Figure 6). Structural parameters of $\mathbf{AgCC}^+$ show slightly longer bond lengths for $O_1{-}N_1$ and $N_2{-}O_2$ than those of **CC-1** but shorter than $P_1{-}O_1$ and $O_2{-}P_2$ bond lengths. Interestingly, $O{=}P_1$, $O{=}P_2$, and $N_1{-}N_2$ bond lengths remain essentially the same.

The effect of Ag(I) on the potential energy surface (PES) of **C** is shown in Figure 7 and Table 5. The binding enthalpy (298 K) of Ag^+ to both P═O oxygen atoms of the bidentate ligand

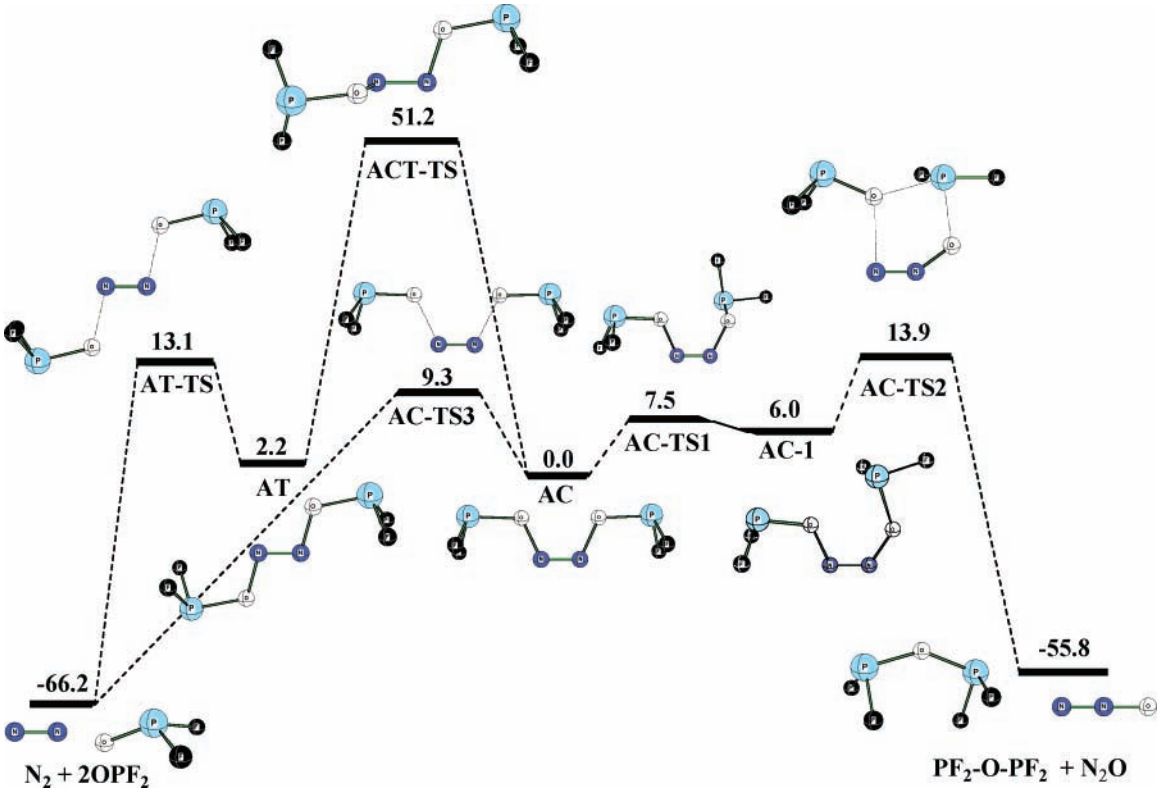

Figure 2. Reaction profiles of free energies for the reaction of **A** in THF solution at the B3LYP/LBS//B3LYP/SBS level.

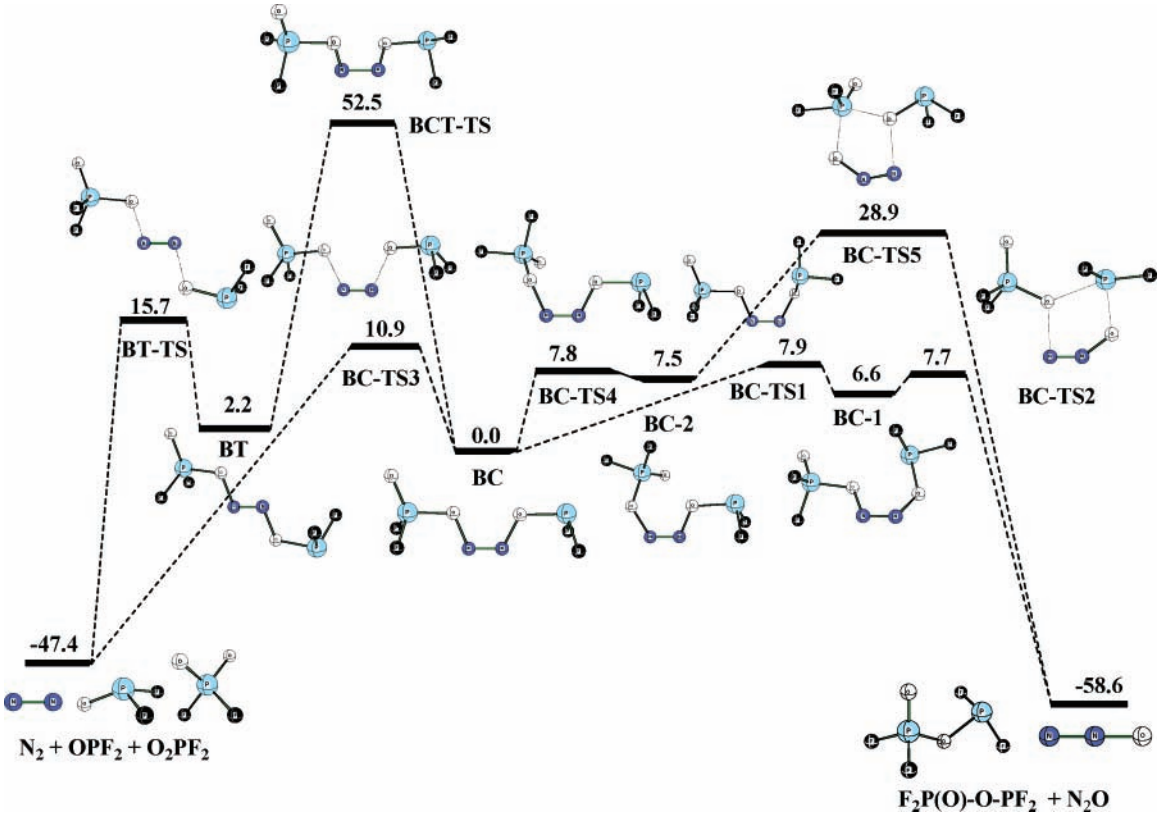

Figure 3. Reaction profiles of free energies for the reaction of **B** in THF solution at the B3LYP/LBS//B3LYP/SBS level.

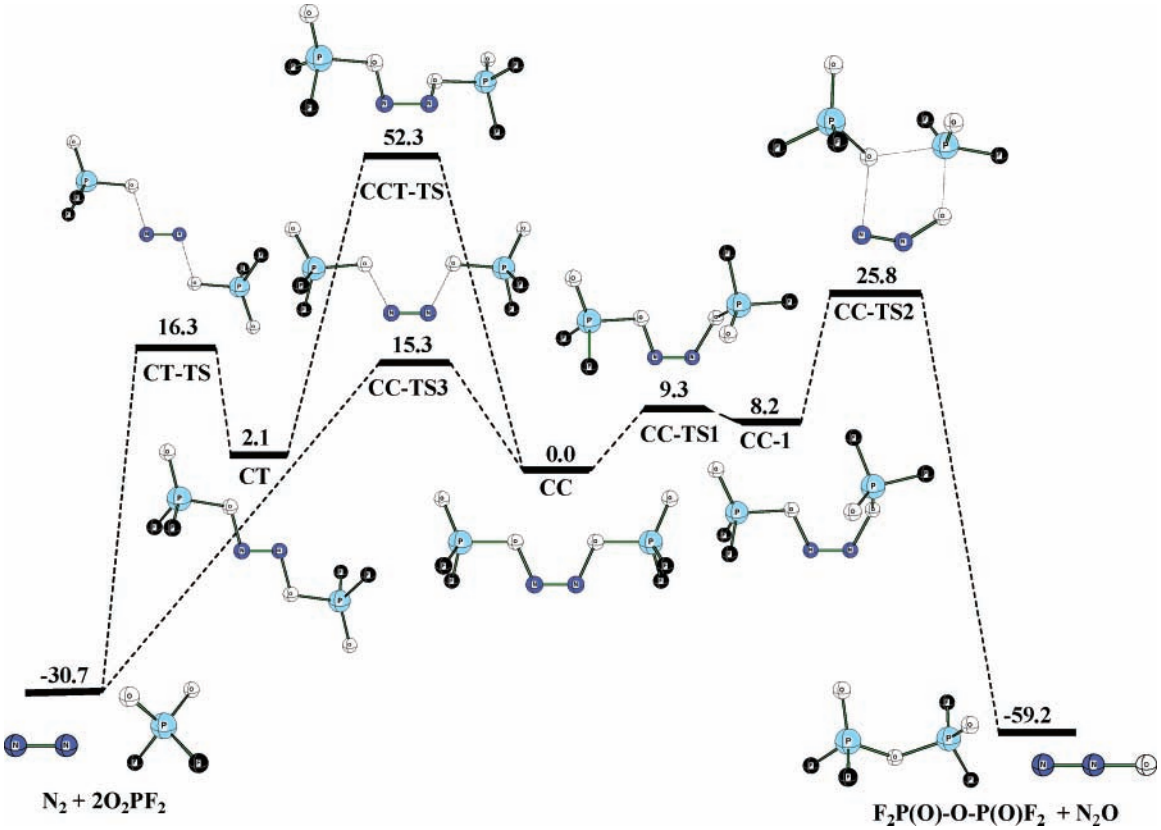

Figure 4. Reaction profiles of free energies for the reaction of **C** in THF solution at the B3LYP/LBS//B3LYP/SBS level.

is 37.8 kcal/mol (Table 5) relative to the lowest conformation (**CC**) of the ligand and 47.4 kcal/mol relative to the less stable **CC-1** conformation. In comparison, the experimental gas-phase binding enthalpy[45] (298 K) of the first two waters to Ag^+ is 58.7 (33.3 + 25.4) kcal/mol. Calculated Ag^+ binding enthalpies to oxygen range from 32 to 38 kcal/mol (water, methanol, ethanol, diethyl ether, and acetone).[46] In THF (which models the $F_2P(O)Br$ neat reaction environment), the Ag^+ cation is predicted to be bound relative to Ag^+ + **CC** by 6.0 kcal/mol in free energy (Figure 7).

TABLE 4: Natural Population Analysis (NPA) Charges for Stationary Points at the B3LYP/SBS Level[a]

	P_1	P_2	N_1	N_2	O_1	O_2	O=P_1	O=P_2	Ag
AC	1.73	1.73	0.13	0.13	−0.70	−0.70			
AC-1	1.75	1.71	0.11	0.18	−0.78	−0.71			
AT	1.73	1.73	0.11	0.11	−0.68	−0.68			
AC-TS1	1.74	1.70	0.14	0.14	−0.72	−0.69			
AC-TS2	1.72	1.76	0.17	0.31	−1.12	−0.48			
AC-TS3	1.80	1.80	0.13	0.13	−0.78	−0.78			
BC	2.64	1.74	0.12	0.15	−0.70	−0.68	−1.02		
BC-1	2.65	1.73	0.11	0.20	−0.79	−0.63	−1.02		
BC-2	2.60	1.75	0.16	0.16	−0.70	−0.69	−1.02		
BT	2.53	1.66	0.10	0.13	−0.64	−0.64	−0.97		
BC-TS1	2.64	1.71	0.13	0.16	−0.72	−0.67	−1.01		
BC-TS2	2.65	1.79	0.19	0.30	−1.07	−0.50	−1.05		
BC-TS3	2.62	1.85	0.13	0.13	−0.72	−0.78	−0.99		
BC-TS4	2.60	1.74	0.14	0.16	−0.71	−0.67	−1.02		
BC-TS5	2.56	1.79	0.29	0.20	−0.49	−1.03	−1.04		
CC	2.63	2.63	0.14	0.14	−0.67	−0.67	−1.01	−0.67	
CC-1	2.62	2.60	0.15	0.17	−0.68	−0.69	−0.99	−1.11	
CT	2.63	2.63	0.11	0.11	−0.65	−0.65	−1.01	−1.01	
CS-TS1	2.62	2.60	0.15	0.16	−0.67	−0.69	−0.99	−1.02	
CS-TS2	2.66	2.56	0.23	0.31	−1.07	−0.48	−1.02	−1.00	
CS-TS3	2.61	2.61	0.14	0.14	−0.69	−0.69	−0.96	−0.96	
AgCC$^+$	2.70	2.69	0.18	0.22	−0.72	−0.70	−1.11	−1.14	0.96
AgCC-TS2$^+$	2.69	2.65	0.33	0.37	−1.19	−0.48	−1.20	−1.03	0.95
AgCC-TS3$^+$	2.67	2.67	0.20	0.20	−0.80	−0.68	−1.04	−1.09	0.95

[a] See Scheme 1 for numbering.

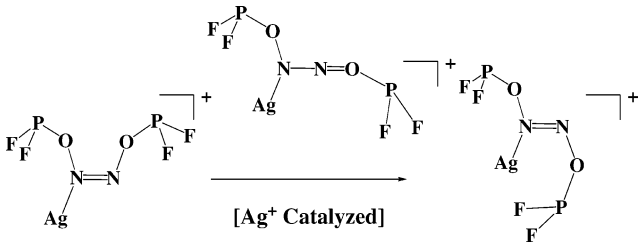

Figure 5. Illustration of possible catalytic effect of Ag^+ on the cis → trans isomerization of $F_2PON{=}NOPF_2$.

The bound Ag^+ has a dramatic effect on the free energies of the two reaction pathways, N_2-producing and N_2O-producing. The bound Ag(I) reduces the free energy barrier of the N_2O-producing pathway from 25.8 to 8.0 kcal/mol. On the other hand, the bound Ag(I) reduces the free energy barrier of the N_2-producing pathway by only 1.7 kcal/mol (15.3 → 13.6 kcal/mol, Figure 7). Thus, the Ag(I) reverses the relative free energies of the two pathways compared to the Ag(I)-free reaction and may explain why the N_2O-producing pathway is observed experimentally.

The relative stabilities of possible radical products including PF_2, OPF_2, and O_2PF_2 were also examined (Table 6). The PF_2 radical has been observed and computed,[47] but the OPF_2 and O_2PF_2 radicals have not yet been reported. Some experimental evidence for the existence of O_2PF_2 has been given.[48] From the first four reaction enthalpies (298 K) in Table 6, it can be seen that the O−P bond enthalpies vary from 70.8 to 96.8 kcal/mol. This variation can be understood from differences in radical stabilization energies (RSE), or, by the fact that the unpaired electron density reorganizes from the nascent radical fragment to the final radical product. From a comparison of the spin densities and NPA charges (Table 7), it is clear that almost all of the unpaired spin density is on phosphorus in PF_2 and OPF_2, while it is distributed between the two oxygen atoms in O_2PF_2. Thus, the initial radical formed by breaking the N−O bond in $N{-}OPF_2$ will undergo significant radical stabilization to form a radical with unpaired spin on the phosphorus center, while the initial radical formed by breaking the O−P or N−O bond in $O{-}PF_2$ or $N{-}OP(O)F_2$ will undergo little radical stabilization.

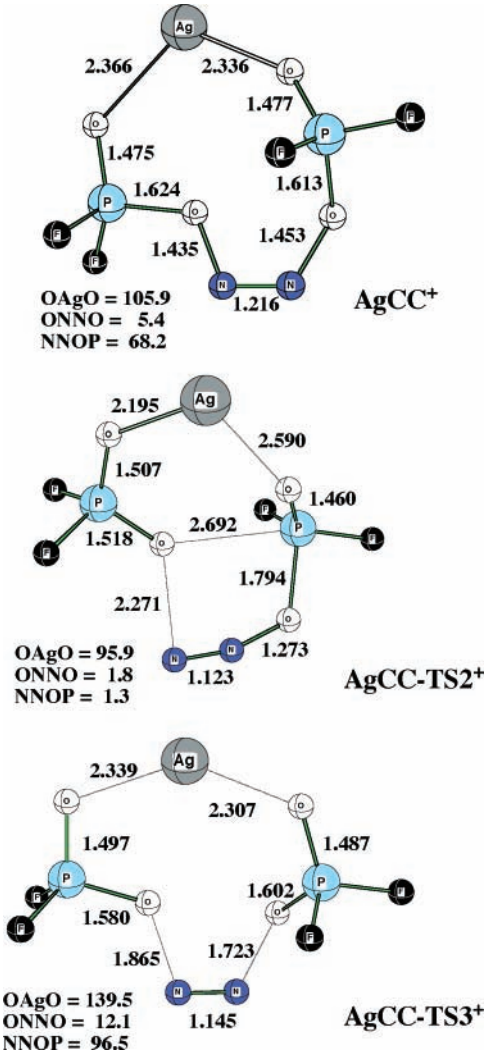

Figure 6. Optimized geometries of $F_2P(O)ON{=}NOP(O)F_2$ with Ag-(I) at the B3LYP/SBS level.

RSE is defined in this work as the enthalpy change of the isodesmic reaction eq 4

$$HO{-}H + XO \rightarrow XO{-}H + OH \qquad (4)$$

$$X = PF_2, OPF_2$$

where RSE = $\Delta H_{rxn} = \Delta H_{products} - \Delta H_{reactants}$. From this isodesmic reaction, the RSE of OPF_2 was determined to be 24.2 kcal/mol, which is much larger than the value for O_2PF_2 (4.2 kcal/mol at the B3LYP/LBS//B3LYP/SBS level including ZPC and C_p corrections to 298 K).

The much larger RSE of OPF_2 compared to O_2PF_2 explains the large change in reaction exothermicities in the N_2-producing pathways of **AC**, **BC**, and **CC** (Tables 2−4: −46.5, −29.4, and −13.9 kcal/mol, respectively). The N_2-producing pathway of **AC** breaks two $N{-}OPF_2$ bonds, compared to one $N{-}OPF_2$ bond for the **BC** reaction and none for the **CC** reaction. The difference in reaction exothermicities ($\Delta\Delta H_{rxn}$) is 17.1 kcal/mol for the **BC**/**AC** reactions and 15.1 kcal/mol for the **CC**/**BC** reactions, which approximately equals the difference between the RSEs of OPF_2 and O_2PF_2 (20.0 kcal/mol).

The variation in the activation enthalpies for the N_2-producing pathway for $XN{=}NX \rightarrow 2X + N_2$, X = OPF_2, $OP(O)F_2$, can also be understood in terms of the RSE of the radicals produced: $^{\bullet}OPF_2$ and $^{\bullet}OP(O)F_2$ (Table 8). When two OPF_2

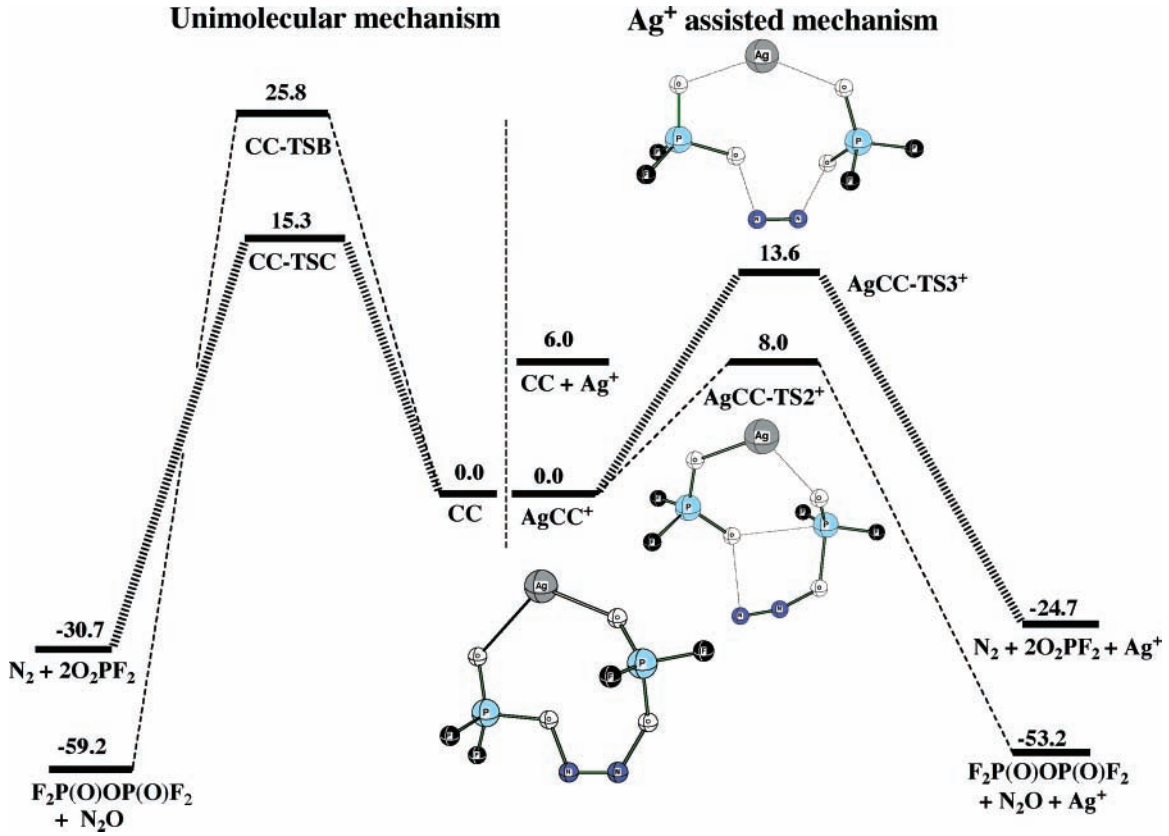

Figure 7. Comparison of the free energy reaction profiles for **C** in THF with **C** catalyzed by Ag(I) in THF.

TABLE 5: Binding Energies, Enthalpies, and Free Energies (kcal/mol) of Ag(I) with $F_2P(O)ON{=}NOP(O)F_2$ [a]

	ΔE_e	ΔH_{0K}	ΔH_{298K}	ΔG_{298K}	ΔG_{THF}[b]
AgCC$^+$	37.9	37.6	37.8	30.1	6.0
AgCC-TS2$^+$	55.3	54.7	54.4	48.4	23.8
AgCC-TS3$^+$	41.8	41.0	41.3	33.2	7.7

[a] Calculated at B3LYP/LBS+CPCM//B3LYP/SBS level. [b] Including solvation free energy calculated by CPCM method in THF.

TABLE 6: Reaction Enthalpies and Free Energies (kcal/mol) for Radical Recombinations[a]

bond energy	ΔE_e	ΔH_{0K}	ΔH_{298K}	ΔG_{298K}	ΔG_{THF}[b]
$PF_2 + OPF_2 \rightarrow F_2P{-}OPF_2$	−72.2	−70.6	−70.8	−58.4	−58.8
$OPF_2 + OPF_2 \rightarrow F_2PO{-}P(O)F_2$	−83.0	−80.7	−81.0	−68.7	−67.7
$PF_2 + O_2PF_2 \rightarrow F_2PO{-}P(O)F_2$	−92.3	−89.5	−89.8	−78.4	−80.5
$OPF_2 + O_2PF_2 \rightarrow F_2P(O)\text{-}OP(O)F_2$	−100.0	−96.5	−96.8	−84.5	−84.8
$OPF_2 + OPF_2 \rightarrow F_2P(O)\text{-}P(O)F_2$	−63.5	−60.8	−61.1	−47.9	−46.0
$OPF_2 + OPF_2 \rightarrow F_2PO{-}OPF_2$	7.2	8.0	8.0	20.6	21.2

[a] Calculated at B3LYP/LBS//B3LYP/SBS level. [b] Including solvation free energy calculated by CPCM method in THF.

TABLE 7: Atomic Mulliken Spin Densities and NPA Charges of Radical Species Calculated at the B3LYP/SBS Level

radical	PF_2		OPF_2		O_2PF_2	
atom	spin density	NPA charge	spin density	NPA charge	spin density	NPA charge
P	1.02	1.17	0.77	2.03	−0.09	2.57
F	−0.01	−0.58	−0.01	−0.55	0.01	−0.54
O			0.25	−0.93	0.53	−0.74

radicals are formed by the N_2-procducing pathway, the activation barrier is smaller than when two O_2PF_2 radicals are produced (12.0 compared to 20.2 kcal/mol, Table 8) due to the much larger RSE of the OPF_2 radicals. Support for this interpretation comes from the experimental activation enthalpies of organic

TABLE 8: Kinetic and Thermodynamic Data (kcal/mol) for the Concerted N_2-Producing Pathway[a]

trans-XN=NX X =	ΔH_a(298 K) N_2-Producing	ΔH_{rxn} (298 K)	RSE[b]
OPF_2	12.0	−48.4	$2{\cdot}24.2 = 48.4$
O_2PF_2	20.2	−15.9	$2{\cdot}4.2 = 8.4$
OR	25−30[c]		∼30[d]

[a] Calculated with respect to the *trans*-hyponitrite isomer. See Tables 1−3. [b] From eq 4. [c] See ref 49 where R=CH_3, CH_3CH_2, $(CH_3)_2CH$, and $(CH_3)_3C$. [d] The RSE for OCH_3 and $OCMe_3$ are computed from eq 4 to be 15.8 and 14.0 kcal/mol, respectively. The N_2-producing pathway would produce two OR radicals which would give a total RSE of about 30 kcal/mol.

hyponitrites RON=NOR, R = CH_3, CH_3CH_2, $(CH_3)_2CH$, $(CH_3)_3C$, which are known to produce N_2 upon decomposition[47] with experimental barriers of 25−30 kcal/mol.[49] The RSEs of RO, R=CH_3, and R=CMe_3 are calculated to be 15.8 and 14.0 kcal/mol, respectively (Table 8). It is probable that the N_2-producing barrier of $F_2PON{=}NOPF_2$ (12.0 kcal/mol, calcd) is lower than the $H_3CON{=}NOCH_3$ and $Me_3CON{=}NOCMe_3$ barriers (25−30 kcal/mol, exptl) due to the larger RSE of OPF_2 compared to OCH_3 and $OCMe_3$ (Table 8).

Conclusion

The reactions of neat F_2PBr and $F_2P(O)Br$ with silver hyponitrite (AgON=NOAg) did not produce the expected phosphorus-containing hyponitrites, $F_2PON{=}NOPF_2$ and $F_2P(O)ON{=}NOP(O)F_2$, but rather N_2O and μ-oxo phosphorus species. A computational study of XON=NOY, X, Y = PF_2, $P(O)F_2$, using density functional theory was carried out to explain the absence of any phosphorus-containing hyponitrites. Single-point energies (B3LYP/6-311+G(2df)//B3LYP/6-31+G(d)) using the CPCM method with the dielectric constant of

THF were used to simulate the experimental environment of neat F_2PBr or $F_2P(O)Br$. Two dissociation pathways, N_2-producing and N_2O-producing, were considered. For $F_2P(O)$-ON═NOPF_2, the N_2O-producing pathway was lower in free energy, while the two pathways were of similar free energy in F_2PON═NOPF_2. For $F_2P(O)ON$═NOP(O)F_2, the N_2-producing pathway was 10.5 kcal/mol lower in free energy, which is in conflict with experiment (only N_2O is produced). The disagreement is removed when the catalytic effect of Ag^+ (present from the silver hyponitrite reactant) is considered. The Ag^+ is predicted to lower the free energy barrier of the N_2O-producing pathway much more than the N_2-producing pathway.

Acknowledgment. Computer time was made available on the Auburn COSAM PRISM cluster.

Supporting Information Available: Spin-squared values at the B3LYP/SBS level, zero-point energies (kcal/mol), heat capacity corrections to 298 K (kcal/mol), entropies (cal/mol·K), free energies of solvation in THF (kcal/mol), and total energies (hartrees) are tabulated in Table S1 (1 pages). Cartesian coordinates of all optimized structures in Tables 1−3 and 5 at the B3LYP/6-31+G(d) level are given in Table S2 (11 pages). This material is available free of charge via the Internet at http://pubs.acs.org.

References and Notes

(1) Hughes, M. N. *Q. Rev. Chem. Soc.* **1968**, *22*, 1.
(2) Kiefer, H.; Traylor, T. G. *Tetrahedron Lett.* **1966**, *7*, 6163.
(3) Arulsamy, N.; Bhole, D. S.; Imonigie, J. A.; Sagan, E. S. *J. Am. Chem. Soc.* **2000**, *122*, 5539.
(4) Kuhn, L.; Lippincott, E. R. *J. Am. Chem. Soc.* **1956**, *78*, 1820.
(5) Rauch, J. E.; Decius, J. C. *Spectrochim. Acta* **1966**, *22*, 1963.
(6) Hughes, M. N. *J. Inorg. Nucl. Chem.* **1967**, *29*, 1376.
(7) McGraw, G. E.; Bernitt, D. L.; Hisatsune, I. C. *Spectrochim. Acta* **1967**, *23A*, 25.
(8) Hughes, M. N.; Stedman, G. *J. Chem. Soc.* **1963**, 2824.
(9) Fraser, R. T. M.; Lee, R. N.; Hyden, K. *J. Chem. Soc. A* **1967**, 741.
(10) Neuman, R. C., Jr.; Bussey, R. J. *J. Am. Chem. Soc.* **1970**, *92*, 2440.
(11) Addison, C. C.; Gamlen, G. A. Thompson, R. *J. Chem. Soc.* **1952**, 338.
(12) Quinga, E. M. Y.; Mendenhall, G. D. *J. Org. Chem.* **1985**, *50*, 2836.
(13) Beck, W.; Engelmann, H.; Smedal, H. S. *Z. Anorg. Allg. Chem.* **1968**, *357*, 134.
(14) Wiberg, V. N.; Bayer, H.; Zeigleder, G. *Z. Anorg. Allg. Chem.* **1979**, *459*, 208.
(15) Brown, R. E.; Mendenhall, G. D.; Bartlett, R. J. *Int. J. Quantum Chem. Symp.* **1987**, *21*, 603.
(16) Quinga, E. M. Y.; Bieker, T.; Dziobak, M. P.; Mendenhall, G. D. *J. Org. Chem.* **1989**, *54*, 2769.
(17) Abata, J. D.; Dziobak, M. P.; Nachbor, M.; Mendenhall, G. D. *J. Phys. Chem.* **1989**, *93*, 3368.
(18) Prinetto, F.; Ghiotti, G.; Nova, I.; Lietti, L.; Tronconi, E.; Forzatti, P. *J. Phys. Chem. B* **2001**, *105*, 12732.
(19) Westerberg B.; Fridell, E. *J. Mol. Catal. A: Chem.* **2001**, *165*, 249.
(20) Al-Ajlouni, A. M.; Gould, E. S *J. Chem. Soc., Dalton Trans.* **2000**, 1239.
(21) Feldmann, C.; Jansen, M. *Angew. Chem., Int. Ed. Engl.* **1996**, *35*, 1728.
(22) Arulsamy, N.; Bohle, D. S.; Imonigie, J. A.; Levine, S. *Angew. Chem., Int. Ed.* **2002**, *41*, 2371.
(23) Poskrebyshev, G. A.; Shafirovich, V.; Lymar, S. V. *J. Am. Chem. Soc.* **2004**, *126*, 891.
(24) Arulsamy, N.; Bohle, D. S.; Imonigie, J. A.; Sagan, E. S. *Inorg. Chem.* **1999**, *38*, 2716.
(25) Brauer, G. *Handbook of Preparative Inorganic Chemistry*; Academic Press: New York, 1963; Vol. 1, p 494.
(26) Parshall, G. W. *Inorganic Synthesis*; McGraw-Hill: New York, 1974; Vol. 15, p 186.
(27) Parry, R. W. *Inorganic Synthesis*; McGraw-Hill: New York, 1970; Vol. 12, p 287.
(28) Reinhardt, H.; Bianchi, D.; Mölle, D. *Chem. Ber.* **1957**, *90*, 1656.
(29) Cavell, R, G. *Can. J. Chem.* **1967**, *45*, 1309.
(30) Magnelli, D. D.; Tesi, G.; Lowe, J. U., Jr.; McQuisition, W. E. *Inorg. Chem.* **1966**, *5*, 457.
(31) Hägele, G.; Kuchen, W.; Steinberger, H. *Z. Naturforsch.* **1974**, *29B*, 349.
(32) Crutchfield, M. M.; Dungan, C. H.; Lechter, J. H.; Mark, V.; Van Wazer, J. R. In *Topics in Phosphorus Chemistry*; Grayson, M., Griffith, E. J., Eds.; Wiley: New York, 1967; Vol. 5, p 281.
(33) Robinson, S. A. *Can. J. Chem.* **1962**, *40*, 1725.
(34) Rudolph, R. W.; Taylor, R. C.; Parry, R. W. *J. Am. Chem. Soc.* **1966**, *88*, 3729.
(35) Frisch, M. J.; Trucks, G. W.; Schlegel, H. B.; Scuseria, G. E.; Robb, M. A.; Cheeseman, J. R.; Montgomery, J. A., Jr.; Vreven, T.; Kudin, K. N.; Burant, J. C.; Millam, J. M.; Iyengar, S. S.; Tomasi, J.; Barone, V.; Mennucci, B.; Cossi, M.; Scalmani, G.; Rega, N.; Petersson, G. A.; Nakatsuji, H.; Hada, M.; Ehara, M.; Toyota, K.; Fukuda, R.; Hasegawa, J.; Ishida, M.; Nakajima, T.; Honda, Y.; Kitao, O.; Nakai, H.; Klene, M.; Li, X.; Knox, J. E.; Hratchian, H. P.; Cross, J. B.; Adamo, C.; Jaramillo, J.; Gomperts, R.; Stratmann, R. E.; Yazyev, O.; Austin, A. J.; Cammi, R.; Pomelli, C.; Ochterski, J. W.; Ayala, P. Y.; Morokuma, K.; Voth, G. A.; Salvador, P.; Dannenberg, J. J.; Zakrzewski, V. G.; Dapprich, S.; Daniels, A. D.; Strain, M. C.; Farkas, O.; Malick, D. K.; Rabuck, A. D.; Raghavachari, K.; Foresman, J. B.; Ortiz, J. V.; Cui, Q.; Baboul, A. G.; Clifford, S.; Cioslowski, J.; Stefanov, B. B.; Liu, G.; Liashenko, A.; Piskorz, P.; Komaromi, I.; Martin, R. L.; Fox, D. J.; Keith, T.; Al-Laham, M. A.; Peng, C. Y.; Nanayakkara, A.; Challacombe, M.; Gill, P. M. W.; Johnson, B.; Chen, W.; Wong, M. W.; Gonzalez, C.; Pople, J. A. *Gaussian 03*, revision B.04; Gaussian, Inc.: Pittsburgh, PA, 2003.
(36) Koch, W.; Holthausen, M. C. *A Chemist's Guide to Density Functional Theory*; Wiley: New York, 2001.
(37) (a) Hay, P. J.; Wadt, W. R. *J. Chem. Phys.* **1985**, *82*, 270. (b) Wadt, W. R.; Hay, P. J. *J. Chem. Phys.* **1985**, *82*, 284. (c) Hay, P. J.; Wadt, W. R. *J. Chem. Phys.* **1985**, *82*, 299.
(38) Schaftenaar, G.; Noordik, J. H. MOLDEN. *J. Comput.-Aided Mol. Des.* **2000**, *14*, 123.
(39) Dolg, M.; Stoll, H.; Preuss, H.; Pitzer, R. M. *J. Phys. Chem.* **1993**, *97*, 5852.
(40) Reed, A.; Curtiss, L. A.; Weinhold, F. *Chem. Rev.* **1988**, *88*, 899.
(41) (a) Barone V.; Cossi, M. *J. Phys. Chem. A* **1998**, *102*, 1995. (b) Cossi, M.; Rega, N.; Scalmani, G.; Barone, V. *J. Comput. Chem.* **2003**, *24*, 669.
(42) The dielectric constant for THF is 7.5. The dielectric constant for liquid O═PCl_3 is 14.0. See http://www.asiinstr.com/dc1.html.
(43) Loechler, E. L.; Schneider, A. M.; Schwartz, D. B.; Hollocher, T. C. *J. Am. Chem. Soc.* **1987**, *109*, 3076.
(44) Hussain, M. A.; Stedman, G.; Hughes, M. N. *J. Chem. Soc. B* **1968**, 597.
(45) Holland, P. M.; Castleman, A. W., Jr. *J. Chem. Phys.* **1982**, *76*, 4195.
(46) (a) Ma, N. L. *Chem. Phys. Lett.* **1998**, *297*, 230. (b) El Aribi, H.; Shoeib, T.; Ling, Y.; Rodriquez, C. F.; Hopkinson, A. C.; Siu, K. W. M. *J. Phys. Chem. A* **2002**, *106*, 2908.
(47) (a) Howe, J. D.; Ashfold, M. N. R.; Hudgens, J. W.; Johnson, R. D., III *J. Chem. Phys.* **1994**, *101*, 3549. (b) Burdet, J. K.; Hodges, L.; Dunning, V.; Current, J. H. *J. Phys. Chem.* **1970**, *74*, 4053. (c) Nelson, W.; Jackel, G.; Gordy, W. *J. Chem. Phys.* **1970**, *52*, 4572. (d) Wei, M. S.; Current, J. H.; Gendell, J. *J. Chem. Phys.* **1970**, *52*, 1592. (e) Hinchliffe, A.; Bounds, D. G. *J. Mol. Struct.* **1979**, *54*, 231.
(48) Eisenberg, M.; Desmarteau, D. D. *Inorg. Chem.* **1972**, *11*, 1901.
(49) Chen, H.-T. E.; Mendenhall, G. D. *J. Am. Chem. Soc.* **1984**, *106*, 6375.